Fast Iterative-Interpolated DFT Phasor Estimator Considering Out-of-band Interference

Jian Song, *Student Member,* Alessandro Mingotti, *Member, IEEE,* Junhao Zhang, *Member, IEEE,*
Lorenzo Peretto, *Senior Member, IEEE,* and He Wen, *Senior Member, IEEE*

Abstract—For interpolated discrete Fourier transform (IpDFT) -based phasor estimators, the Out-of-band interference (OOBI) test is among the most challenging ones. The typical iterative-interpolated DFT (i-IpDFT) phasor estimator utilizes a two-step iterative framework to eliminate the effects of the negative frequency and OOBI. However, the speed of estimation is limited by the adopted frequency estimator and the redundant iterations. To this end, this paper proposes a fast i-IpDFT (FiIpDFT) method for the phasor estimation of an OOBI contaminated signal, which utilizes the three-point IpDFT (I3pDFT) technique. The proposed method first applies a non-iterative frequency, amplitude, and phase estimator to eliminate the negative frequency interference. Then, a straightforward formula and two-stop criterion are introduced to reduce the computational burden of the OOBI elimination process. The accuracy and effectiveness of the proposed FiIpDFT method are validated by simulations. These are designed, under steady and dynamic conditions, according to the requirements of the Standard IEC/IEEE 60255-118-1.

Index Terms—Phasor estimation, Interpolated discrete Fourier transform (IpDFT), out-of-band interference (OOBI) test, phasor measurement units (PMUs), IEC/IEEE 60255-118-1.

I. INTRODUCTION

SINCE reducing carbon emissions has become consensus and all countries in the world are taking countermeasures, numerous distributed energy resources (e.g., photovoltaic, wind plants) are being connected to power systems [1]. In these circumstances, the power waveform suffers from fast dynamics and Out-of-band interference (OOBI) which deteriorate the measurement accuracy of phasor estimators. Phasor measurement units (PMUs) are key instruments that are employed in smart grids to estimate amplitude, phase, frequency, and rate of change of frequency (ROCOF) of voltage and current waveforms [2]. All estimation results are synchronized to the universal coordinated time (UTC). To characterize the behavior of PMUs, the IEEE Standard C37.118.1 [3, 4] and its latest version IEC/IEEE 60255-118-1 [5], briefly IEEE Std, specify two different performance classes:

the P-class is designed for fast response applications while the M-class is preferred for high precision applications. Both P- and M-class PMU are primarily evaluated in line with three indicators, i.e., total vector error (TVE), frequency error (FE), and ROCOF error (RFE), whose limits are indicated in IEEE Std under the different test conditions.

To track the fast dynamics of modern power signals, many methods for phasor estimation have been designed. The aim is to reduce the measurement reporting latency. In literature, many existing estimators achieve an acceptable measurement latency using the Taylor Weighted Least Squares (TWLS) based method [6-8]. It represents a phasor as a time-varying function and reduces the OOBI infiltration with windowing. To achieve high accuracy and low latency at the same time, TWLS-based methods generally require another algorithm. This is applied to the signal before the TWLS to obtain the power frequency value [8-12]. In [8], the interpolated discrete Fourier transform (IpDFT) is used to extend the TWLS (GTWLS) for resisting frequency deviation and the second harmonic interference. In this way, the GTWLS's behavior has been enhanced, especially under frequency deviation conditions. As extensions of TWLS and GTWLS, [9] and [13] propose low-complexity procedures to reduce the computational burden; hence, applicable in real-time low-cost applications. However, GTWLS and its extensions still suffer the OOBI (i.e., interharmonic nearby the fundamental).

To address the OOBI problem, [10] and [14] (light version of [10]) adopt the compressive sensing instead of the IpDFT. Such a technique aims to estimate the frequencies of the fundamental, the harmonics, and the interharmonics simultaneously. Then, the frequencies are the input of a Taylor-Fourier multifrequency (TFM) model, which can accurately estimate a phasor within five nominal cycles (i.e., 100 ms in 50 Hz system). Conversely from [10] and [14], [12] (TWLSMP) employs the matrix pencil algorithm to estimate rough frequencies, which leads high accuracy estimation results within three nominal cycles (i.e., 60 ms in 50 Hz system). However, its computational burden sharply increases with the number of frequency components (interharmonics or harmonics). The high computational burden of the TWLSMP makes it unsuitable for being implemented in low-cost embedded devices.

Considering the computational burden, most of the existing phasor estimators are based on the IpDFT algorithm [15-17]. It is computationally efficient thanks to the fast Fourier transform (FFT) technique [18]. However, traditional IpDFT-based algorithms suffer from several problems due to the static signal model, the finite frequency resolution, and spectral leakage

Jian Song, Junhao Zhang, and He Wen are with the College of Electrical and Information Engineering, Hunan Province Key Laboratory of Intelligent Electrical Measurement and Application Technology, Hunan University, Changsha 410082, China (e-mail: songjian1705@126.com; luoyzjh@163.com; he_wen82@126.com).

Alessandro Mingotti and Lorenzo Peretto are with the Department of Electric, Electronic and Information Engineering "G.Marconi," University of Bologna, 40136 Bologna, Italy (e-mail: alessandro.mingotti2@unibo.it; lorenzo.peretto@unibo.it).

effects [19-22]. The effects of off-nominal frequency deviation on IpDFT-based algorithms are investigated in [15]. It has been demonstrated that the infiltration of the image of the fundamental component, caused by frequency deviation, impacts the estimator's accuracy. This impact is especially severe in the case of a short observation window (e.g., single cycle). Within this context, the enhanced IpDFT (e-IpDFT) [16] utilizes P iterations to mitigate the effect of the spectral leakage produced by the negative image of the fundamental. However, the e-IpDFT still cannot fully satisfy the requirement of the M-class PMUs within a short observation window (e.g., less than five cycles, OOBI test). The Iterative-IpDFT (i-IpDFT) [17] adds another iterative routine (Q iterations) on the e-IpDFT to estimate and compensate for the effects of the spectral interference produced by OOBI. In this way, i-IpDFT algorithm achieves a minimum window length equal to three nominal cycles. However, the i-IpDFT's behaviors, i.e., accuracy and speed of estimation, is limited by the adopted frequency, amplitude, and phase estimator (AI3pDFT, reported in [23]) under the OOBI conditions.

This paper provides a solution to the above problems by proposing a fast estimator, called fast i-IpDFT (FiIpDFT), that can greatly reduce the computational burden by using a non-iterative frequency, amplitude, and phase estimator and a two-stop criterion. The FiIpDFT results from an extension of the i-IpDFT presented in [17], and it outperforms the i-IpDFT in the most critical testing conditions reported in the IEEE Std. In the OOBI tests, the computational efficiency of the proposed technique is at least 8 times higher than the i-IpDFT one. Since the FiIpDFT is particularly effective under the OOBI condition, it should be suitable for PMUs requiring both low-cost and low reporting latency.

The rest of the paper is structured as follows: Section II presents the limitations of the i-IpDFT and the motivation for this work, Section III summarizes the signal model, recalls the procedure of the adopted estimator, and describes the proposed FiIpDFT algorithm. Section IV presents the results of the proposed method validation tests (according to IEEE Std). Finally, in Section V, the main conclusions are summarized.

II. LIMITATIONS OF THE I-IpDFT & MOTIVATIONS

During each iteration of the i-IpDFT method [17], the OOBI, i.e., subharmonic or interharmonic nearby the fundamental, is estimated and then subtracted from the original DFT spectrum. For an interfering frequency within 10 Hz and 25 Hz, a three cycles window of the 50 Hz signal corresponds to a 3/5 and 3/2 cycles window for each tone, respectively. As shown in Fig. 1, the frequency estimator used in the e-IpDFT and i-IpDFT, i.e., FreqEst1 [23], has a very large error in the case of such a short observation window. Although estimation errors can be continuously reduced by P iterations in the e-IpDFT, the computational burden grows with the number of iterations. Moreover, when the interharmonic tone's frequency is 10 Hz, the e-IpDFT's maximum estimation error is 10 mHz even if 40 iterations are used. In addition, a larger interharmonic estimation error in the e-IpDFT leads to more iterations (bigger Q) required to reach a sufficient estimation accuracy in the
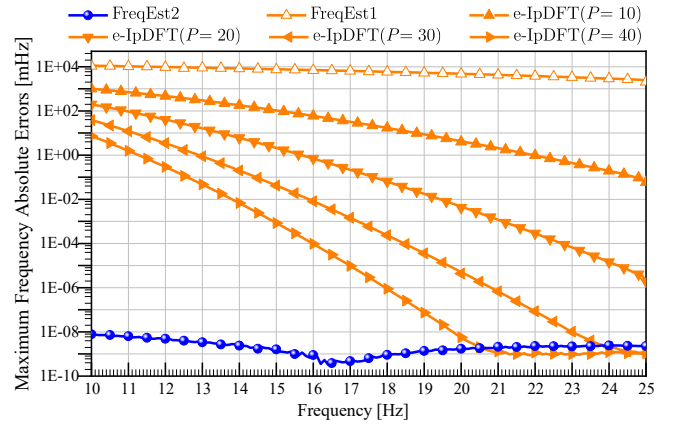

Fig. 1. Maximum frequency absolute errors from different frequency estimators. The FreqEst1 [23] refers to the frequency estimator used in the e-IpDFT and the i-IpDFT, while the FreqEst2 [24] refers to the frequency estimator adopted in this paper (FiIpDFT). f_s = 50 kHz, 3000 samples.

i-IpDFT. Therefore, the total number of iterations, i.e., $(P+1)\cdot(2\cdot Q+1)$, of the i-IpDFT can be a huge number if high measurement accuracy is required.

Fortunately, a novel and robust frequency estimator, briefly FreqEst2, is reported in [24]. As shown in Fig. 1, FreqEst2 (without iteration) outperforms all other methods (which use up to 40 iterations) when a short observation window is adopted (e.g., range in [3/5, 3/2] cycles). Its excellent performance implies it can be applied for phasor estimation under OOBI conditions. The proposed FiIpDFT is a two-step procedure for phasor parameters estimation. In the first step, a robust amplitude and phase estimator is proposed, which is not affected by the negative frequency of the fundamental. The proposed amplitude and phase estimator and FreqEst2 together are called RI3pDFT. Benefiting from the fact that the RI3pDFT does not require iterations to eliminate the spectral leakage effect of the negative image, the RI3pDFT has a lighter computational complexity compared with the e-IpDFT. In the second step, an iterative routine is adopted to mitigate the effects of OOBI if it is detected. Differently from the i-IpDFT, a simplified and efficient formula, which is used to reconstruct the DFT bins, is introduced first in the FiIpDFT. An indicator is then designed to determine whether to stop iterating to avoid redundant computation in each estimate. By optimizing each step in the iterative process, the estimation speed can be greatly improved, especially under OOBI conditions.

III. PROPOSED PHASOR ESTIMATOR

A. Signal Model and Windowed DTFT

As known, the discrete expression of the standard power signal with N samples is:

$$x(n) = x(t)\big|_{t=nT_s} = A_1 \cos\left(2\pi f_1 n T_s + \phi_1\right), \quad n \in [0, N-1] \quad (1)$$

where f_1, A_1, and ϕ_1 are, respectively, the frequency, amplitude, and phase of the power signal. $T_s = 1/f_s$ is the sampling interval, and f_s is the sampling rate.

To suppress the spectral leakage, the signal $x(n)$ is weighted with a time domain window $w(n)$, i.e., $x_w(n) = x(n)w(n)$. Thus,

the discrete-time Fourier transform (DTFT) of the windowed input signal is:

$$X_w(k) = \frac{A_1}{2}\left[W(k-v)e^{j\phi_1} + W(k+v)e^{-j\phi_1}\right], \quad k \in [0, N-1] \quad (2)$$

where k is the index of DFT bins, $v = f_1 N / f_s$ represents the normalized value corresponding to the frequency of the input signal, and $W(\ )$ is the DTFT of the window $w(\ )$.

Among the numerous window functions, the Hanning window has been proven to perform well for phasor estimation since it has the good tradeoff between the main-lobe width and sidelobe levels [17, 25]. Hence, this work adopts the Hanning window $w_H(n)$ to reduce the effects of spectral leakage, where $w_H(n)$ is defined as:

$$w_H(n) = 0.5 \cdot (1 - \cos(2\pi n / N)), \quad n \in [0, N-1]. \quad (3)$$

For $N \gg 1$, the DTFT of the Hanning window $w_H(n)$ can be approximated by [19]:

$$W_H(\lambda) = \frac{N \sin(\pi\lambda)}{2\pi\lambda(1-\lambda^2)} e^{-j\pi\lambda}, \quad \lambda \in [0, N), \quad (4)$$

where λ is the normalized frequency expressed in bin.

B. The Proposed RI3pDFT Method

In this subsection, the implementation procedure of the proposed P-class phasor estimator is described, along with theoretical and other details. The steps are divided into two stages: first, a three-point IpDFT algorithm (I3pDFT) [24] is introduced to estimate the frequency of the power signal. This frequency estimator effectively removes the interference produced by the negative image. Second, a novel amplitude and phase estimation method is proposed to estimate the phasor in an accurate and fast way.

1) Frequency Estimation Based on I3pDFT Method

In the first stage, the frequency of the input signal is estimated by using I3pDFT technique. If the Hanning window is adopted, the normalized frequency of the input signal can be estimated by interpolation of three DFT bins with the largest magnitudes as [24]:

$$\hat{v} = \sqrt{k_m^2 + \text{real}(\eta)}, \quad (5)$$

where k_m is the index of the highest bin and:

$$\eta = \frac{4\left[(k_m+1)X_w(k_m+1) + X_w(k_m) - (k_m-1)X_w(k_m-1)\right]}{\left(X_w(k_m+1) - 2X_w(k_m) + X_w(k_m-1)\right)}. \quad (6)$$

Then, the frequency of the input signal can be estimated as:

$$\hat{f}_1 = \hat{v} \cdot f_s / N. \quad (7)$$

2) The Proposed Amplitude and Phase Estimator

In the second stage, an accurate amplitude and phase estimator is designed using the estimated normalized frequency $\hat{v}$ in (5) and the conjugation property of equation (2). For the highest DFT bin, equation (2) can be rewritten as:

$$X_w(k_m) = W_H(k_m - \hat{v})P_1 + W_H(k_m + \hat{v})P_1^*, \quad (8).$$

where $P_1 = \frac{1}{2}A_1 e^{j\phi_1}$ refers to the phasor defined in IEEE Std [5] and P_1^* is the conjugate of P_1.

Based on Euler formula, equation (4) can be rewritten as:

$$W_H(\lambda) = D(\lambda)\cos(\pi\lambda) - jD(\lambda)\sin(\pi\lambda), \quad (9)$$

where:

$$D(\lambda) = \frac{N \sin(\pi\lambda)}{2\pi\lambda(1-\lambda^2)}. \quad (10)$$

Let $P_1 = P_{1\text{-r}} + jP_{1\text{-i}}$, $P_1^* = P_{1\text{-r}} - jP_{1\text{-i}}$, $X_w(k_m) = X_r + jX_i$, and by substituting (9) and (10) into (8), one obtain:

$$X_r + jX_i = (D_1 - jD_2)(P_{1\text{-r}} + jP_{1\text{-i}}) + (D_3 - jD_4)(P_{1\text{-r}} - jP_{1\text{-i}})$$

$$= \begin{pmatrix} D_1 + D_3 \\ D_2 - D_4 \end{pmatrix}^T \begin{pmatrix} P_{1\text{-r}} \\ P_{1\text{-i}} \end{pmatrix} + j\begin{pmatrix} -D_4 - D_2 \\ D_1 - D_3 \end{pmatrix}^T \begin{pmatrix} P_{1\text{-r}} \\ P_{1\text{-i}} \end{pmatrix}, \quad (11)$$

where $(\ )^T$ denotes the transpose operator and:

$$\begin{aligned} D_1 &= D(k_m - \hat{v})\cos(\pi(k_m - \hat{v})) \\ D_2 &= D(k_m - \hat{v})\sin(\pi(k_m - \hat{v})) \\ D_3 &= D(k_m + \hat{v})\cos(\pi(k_m + \hat{v})) \\ D_4 &= D(k_m + \hat{v})\sin(\pi(k_m + \hat{v})) \end{aligned} \quad (12)$$

It is worth noting that the real and imaginary parts of both sides of the equation (11) are independently equal, so it can be rearranged as:

$$\begin{pmatrix} X_r \\ X_i \end{pmatrix} = \begin{pmatrix} D_1 + D_3 & D_2 - D_4 \\ -D_4 - D_2 & D_1 - D_3 \end{pmatrix}\begin{pmatrix} P_{1\text{-r}} \\ P_{1\text{-i}} \end{pmatrix}. \quad (13)$$

By solving the above linear equation in two unknowns, the real and imaginary parts of the phasor can be determined from:

$$\begin{cases} \hat{P}_{1\text{-r}} = \dfrac{X_r(D_1 - D_3) - X_i(D_2 - D_4)}{(D_1 + D_3)(D_1 - D_3) + (D_2 - D_4)(D_4 + D_2)} \\ \hat{P}_{1\text{-i}} = \dfrac{X_r(D_2 + D_4) + X_i(D_1 + D_3)}{(D_1 + D_3)(D_1 - D_3) + (D_2 - D_4)(D_4 + D_2)} \end{cases}. \quad (14)$$

Finally, the phasor, amplitude, and initial phase are estimated as:

$$\hat{P}_1 = \hat{P}_{1\text{-r}} + j \cdot \hat{P}_{1\text{-i}} \quad (15)$$

$$\hat{A}_1 = 2\sqrt{\left(\hat{P}_{1\text{-r}}\right)^2 + \left(\hat{P}_{1\text{-i}}\right)^2} \quad (16)$$

$$\hat{\phi}_1 = \arctan\left(\frac{\hat{P}_{1\text{-i}}}{\hat{P}_{1\text{-r}}}\right), \quad (17)$$

and the ROCOF is calculated using the backward first-order approximation of a first-order derivative:

$$\text{ROCOF}(n) = \left|\hat{f}_1(n) - \hat{f}_1(n-1)\right| \cdot F_r, \quad (18)$$

where F_r is the reporting rate of PMU, $\hat{f}_1(n-1)$ and $\hat{f}_1(n)$ represent the estimated fundamental frequencies at two successive reporting frames.

C. The FiIpDFT Phasor Estimator

Although the method reported in the previous subsection fully satisfies the requirements of P-class PMUs within three nominal cycles, it produces inaccurate and unreliable results under OOBI tests when a short observation window is adopted. Here, an iterative routine is introduced to eliminate the effects of spectral leakage generated by an interfering tone close to the fundamental.

1) Signal Model in the Presence of Interfering Tone

Considering the effect of a generic interfering tone, the input signal can be regarded as the sum of a fundamental and an interfering tone:

$$x(n) = A_1 \cos\left(2\pi f_1 n T_s + \phi_1\right) + A_i \cos\left(2\pi f_i n T_s + \phi_i\right), \quad (19)$$

and its windowed DFT spectrum can be modeled as the sum of the fundamental and the interfering tone:

$$X_w(k) = X_{1w}(k) + X_{iw}(k)$$
$$= \frac{1}{2}\left[W(k - v_1)P_1 + W(k + v_1)P_1^*\right], \quad (20)$$
$$+ \frac{1}{2}\left[W(k - v_i)P_i + W(k + v_i)P_i^*\right]$$

where v_i is the normalized frequency of the interfering tone, $P_i = \frac{1}{2}A_i e^{j\phi_i}$ refers to the interharmonic phasor or harmonic phasor corresponding to the interfering tone.

2) Interference Elimination Framework Based on Iterations

To eliminate the effects of spectral leakage generated by an interfering tone close to the fundamental, an iterative routine is introduced. In fact, the proposed FiIpDFT method follows the same framework as the i-IpDFT method [17] to eliminate the effects of a generic interfering one. Furthermore, the two-stop criterion is designed to guarantee feasibility and efficiency. The pseudocode of the proposed FiIpDFT method is presented in Table I. The first steps (lines 1 to 4) of the FiIpDFT aim at determining whether an iterative procedure is required. The rough contribution of the fundamental component, i.e., $\hat{X}_{1w}^0(k)$ in line 3, to the original DFT bins of the windowed input signal is estimated by using the proposed RI3pDFT and formula (2). The estimated results are then subtracted from the original DFT bins to produce a remainder, i.e., $X_w(k) - \hat{X}_{1w}^0(k)$. In general, the remainder mainly correspond to the contribution of the interfering tone. The ratio of spectral energy of the remainder to the original DFT bins, defined in formula (21), is used to determine whether the iterative routine is active or not.

$$E_n = \frac{E\left[X_w(k) - \hat{X}_{1w}^0(k)\right]}{E[X_w(k)]} = \frac{\sum_{k=0}^{K}\left|X_w(k) - \hat{X}_{1w}^0(k)\right|^2}{\sum_{k=0}^{K}|X_w(k)|^2} > \lambda, \quad (21)$$

where λ and K are the threshold and the number of the computed DFT bins, respectively. The rationale behind the selection of λ and K has been reported in [17]. In brief, $\lambda = 3.3 \cdot 10^{-3}$ and $K = 11$ are appropriate when the sampling rate and window length are set as 50 kHz and three nominal cycles, respectively.

If E_n exceeds λ, it means that at least one interfering tone exists, and the iterative routine must be activated. In such a case, the proposed RI3pDFT is used to estimate the parameters $\{\hat{v}_i^q, \hat{P}_i^q\}$ of the interfering tone (line 6). The $\{\hat{v}_i^q, \hat{P}_i^q\}$ are used to reconstruct the spectrum of the interfering tone (line 7) that are then subtracted from the original DFT bins, obtaining the remainder $X_w(k) - \hat{X}_{iw}^q(k)$ that does not contain the interfering

TABLE I THE PSEUDOCODE OF THE PROPOSED FiIpDFT METHOD

Input: $x_w(n)$, Q, K, λ, and ξ.

1. $X_w(k) = \text{FFT}[x_w(n)]$

2. $\{\hat{v}_1^0, \hat{P}_1^0\} = \text{RI3pDFT}[X_w(k)]$

3. $\hat{X}_{1w}^0(k) = W_H(k - \hat{v}_1^0)\hat{P}_1^0 + W_H(k + \hat{v}_1^0)\hat{P}_1^{0*}$

4. **if** $\sum_{k=0}^{K}\left|X_w(k) - \hat{X}_{1w}^0(k)\right|^2 > \lambda \cdot \sum_{k=0}^{K}|X_w(k)|^2$

5.   **for** $q = 1 \rightarrow Q$ @ **stop criterion 1:** Q

6. $\{\hat{v}_i^q, \hat{P}_i^q\} = \text{RI3pDFT}[X_w(k) - \hat{X}_{1w}^{q-1}(k)]$

7. $\hat{X}_{iw}^q(k) = W_H(k - \hat{v}_i^q)\hat{P}_i^q + W_H(k + \hat{v}_i^q)\hat{P}_i^{q*}$

8. $\{\hat{v}_1^q, \hat{P}_1^q\} = \text{RI3pDFT}[X_w(k) - \hat{X}_{iw}^q(k)]$

9. $\hat{X}_{1w}^q(k) = W_H(k - \hat{v}_{1w}^q)\hat{P}_1^q + W_H(k + \hat{v}_1^q)\hat{P}_1^{q*}$

10.   **if** $\text{abs}[\hat{f}_1^q - \hat{f}_1^{q-1}] < \xi$ **break** @ **stop criterion 2:** ξ

11.   **end for**

12. **end if**

Output: $\hat{v}_1^q$ and $\hat{P}_1^q$ correspond to the fundamental.

tone (line 8). Finally, the proposed RI3pDFT leading to a more accurate estimation of the fundamental parameters $\{\hat{v}_1^q, \hat{P}_1^q\}$. Unlike the i-IpDFT, the proposed FiIpDFT adopts an additional stop criterion (line 10) to reduce superfluous and unnecessary iterations. If $\nabla \hat{f}_1^q$ is defined as the absolute difference between two consecutive estimated values of the f_1, the two-stop criterion of the proposed method perform the iterative routine until $\nabla \hat{f}_1^q$ is less than ξ or q is equal to Q. This leads to a lower computation burden in most cases, which is an advantage for a low-cost PMU. The detailed explication will be addressed in the next subsection.

D. Two-Stop Criterion of Proposed FiIpDFT Method

In the case of OOBI, for each frequency of the interharmonic tone, a different number of iterations is necessary to achieve the required accuracy. Fig. 2 depicts the curves of the maximum required iteration number q_{max} under different conditions. The reported q_{max} values are the maximum among the estimations computed by shifting the observation window sample by sample. The overall length of the tested OOBI signal is 250
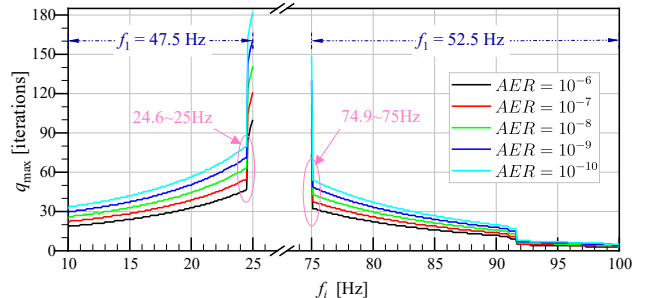

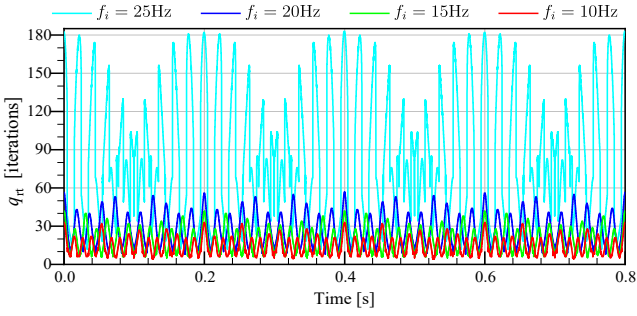Fig. 2. Max required iteration numbers of FiIpDFT in the OOBI tests.

Fig. 3. Required number of iterations q_{rt}, as a function of time: $f_1 = 47.5$ Hz, $AER = 10^{-10}$ Hz; $f_s = 50$ kHz, $T = 60$ ms, and $RR = 50$ kHz.

nominal cycles (i.e., 5 s). Fig. 2 shows that more iterations are required if a lower absolute error requirement (AER) of the fundamental frequency is specified. In addition, more iterations are obviously needed when the frequency of the interfering tone is closer to the fundamental, especially for $24.6 \sim 25$ Hz. This is because the proposed RI3pDFT performs well when a sine-wave with a short length is estimated. Thus, the worst interference between the fundamental and the sub-harmonic occurs when $f_i = 25$ Hz, and the required number of iterations only relates the phases of the fundamental and 25 Hz interfering tone.

Fig. 3 reports the required number of iterations, i.e., q_{rt}, as a function of time, when the AER of f_1 is required to be less than 10^{-10} Hz. It can be seen that q_{rt} changes periodically with time (i.e., initial phase of the estimated observation window), and the maximum values of q_{rt} occurs every 200 ms. By extracting the initial phase values from the observation window which required the maximum iterations, the input signal representing the worst case can be given as:

$$x(n) = \cos(2 \cdot 47.5\pi n T_s + 0.1861\pi)$$
$$+ 0.1\cos(2 \cdot 25\pi n T_s + 0.5190\pi), \quad n \in [1,3000] \tag{22}$$

Moreover, q_{rt} is lower when the interfering tone frequency is lower than 24 Hz. The results in Fig. 2 and Fig. 3 reveal that there will be too many redundant iterations if Q is set to a large and fixed value, which leads to a huge waste of computing resources. Therefore, it is meaningful to design an effective stop criteria other than Q.

Then a heuristic test is conducted to find an effective stop criterion. The worst case is analysed under different noise level conditions. Fig. 4 shows that the absolute error of the estimated f_1, $\Delta \hat{f}_1^q = |\hat{f}_1^q - f_1|$, decrease with the increase of the number of iterations, and so does the absolute difference between two consecutive values of the estimated f_1, i.e., $\nabla \hat{f}_1^q = |\hat{f}_1^q - \hat{f}_1^{q-1}|$. However, $\Delta \hat{f}_1^q$ will be reduced to a limit value after a certain number of iterations according to different noise levels. For example, $\Delta \hat{f}_1^q$ corresponding to 40 dB no longer decreases after 50 iterations. This means that the estimation accuracy of f_1 cannot be improved with further iterations. Hence, the first stop criterion for the FiIpDFT could be set as $Q \le 50$. Meanwhile, Fig. 4 also indicates the minimum number of iterations required by the FiIpDFT to satisfy the IEEE requirements in the worst case. It can be seen that the required iterations should be equal
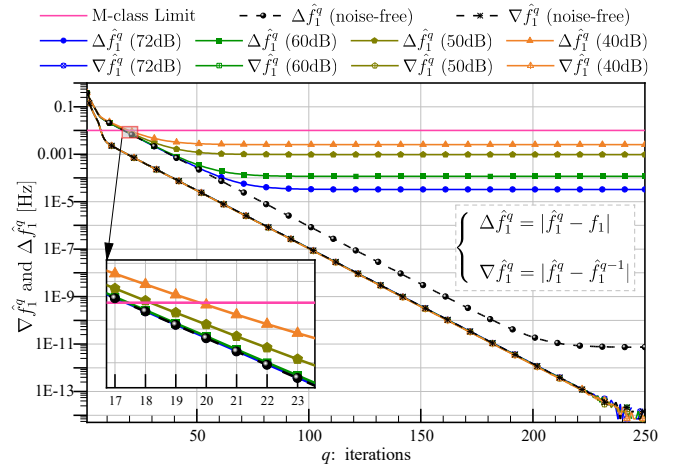

Fig. 4. Absolute error $\Delta \hat{f}_1^q$ and absolute difference $\nabla \hat{f}_1^q$ of the estimated fundamental frequency f_1, as a function of q, in the worst case.

or greater than 18 when the signal-to-noise ratio (SNR) is greater than 50 dB. Consequently, the first stop criterion for the FiIpDFT (i.e., the value of Q) can be chosen between 18 and 50.

Another interesting result is that the curves of $\nabla \hat{f}_1^q$ corresponding to different noise levels in Fig. 4 overlap. This indicates that although $\nabla \hat{f}_1^q$ decreases with the increase of the number of iterations, its downward trend is independent of the noise level. Such a characteristic makes $\nabla \hat{f}_1^q$ another appropriate indicator for stopping the iterative routine. The curves of the $\nabla \hat{f}_1^q$ in Fig. 4 only represent results in the worst scenario. Hence, the value of $\Delta \hat{f}_1^q$ corresponding to 72 dB almost do not decrease after 100 iterations. Meanwhile, the $\nabla \hat{f}_1^q$ is equal to $1.1 \cdot 10^{-7}$ Hz when q is equal to 100. Thus, the second stop criterion for the proposed FiIpDFT method is set as $\xi = 1 \cdot 10^{-7}$. In general, the value of $\nabla \hat{f}_1^q$ decline more quickly than in the worst situation. Hence, the number of iterations that make $\nabla \hat{f}_1^q$ less than $1 \cdot 10^{-7}$ is very small, far less than 18 or 50, especially when f_i is lower than 24.5 Hz or greater than 74.8 Hz.

E. Differences Between the FiIpDFT and the i-IpDFT

The differences between the FiIpDFT and the i-IpDFT are summarized as follows. First, the FiIpDFT adopts the proposed RI3pDFT method to estimate parameters of the frequency component. Comparing with the e-IpDFT used in the i-IpDFT, the RI3pDFT offers a more accurate and faster estimation without iteration. Second, a straightforward formula (4) is applied to reduce the computation burden for the reconstruction of the DFT spectrum in each iteration. Finally, the two-stop criterion is designed in the FiIpDFT to avoid the redundant iterations of the OOBI elimination process.

IV. PERFORMANCE CHARACTERIZATION

In this section, simulations are conducted in MATLAB to analyze the performance of the proposed method. Firstly, the behavior of the amplitude and phase estimator is investigated in terms of mean square error (MSE). Secondly, the performance of the FiIpDFT is characterized in terms of TVE, FE, and RFE. Finally, the computational complexity of the FiIpDFT is analyzed by means of theory and simulations.

A. Behavior of The Proposed Amplitude and Phase Estimator

In addition to the efficient frequency estimator FreqEst2, also the proposed amplitude and phase estimator plays an important role. In fact, it allows the RI3pDFT to eliminate the interference from the fundamental image component without any iteration. In this subsection, the behavior of the proposed amplitude and phase estimator is investigated under short signals and different noise levels. The accuracy of the proposed estimator are compared with those of the PSF-IpDFTc method [26], the IpDFTc method [27, 28], the AI3pDFT method [23], and the e-IpDFT method [16]. It is worth noting that the PSF-IpDFTc method attains the Cramér-Rao Lower Bound (CRLB) for amplitude and phase estimation when the observation window is greater than 1 sine-wave cycle. Moreover, the MSE is used as an evaluation parameter and compared to the related CRLB. To fairly evaluate the behavior of those methods, the frequency of the estimated signal is assumed to be known. The amplitude of the test signal is 1 p.u. while the initial phase is set as a random value between 0 and 2π rad. For each test, 10000 runs of 3000 samples and f_s = 50 kHz are considered.
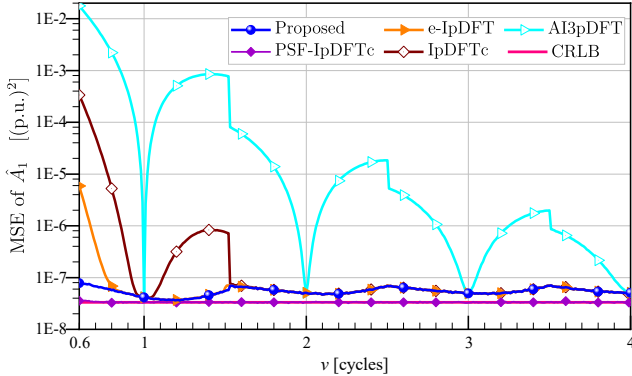

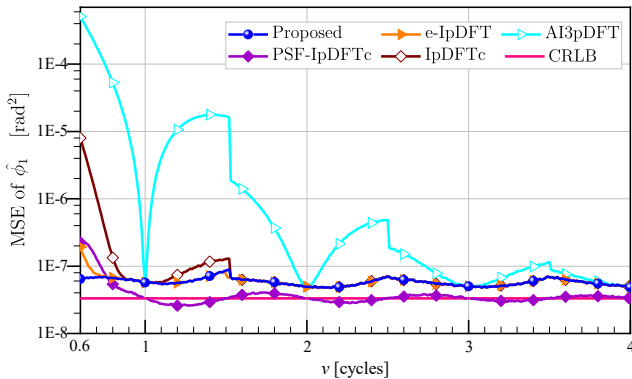Fig. 5. MSEs of $\hat{A}_1$ when SNR = 40 dB, as a function of the v.

Fig. 6. MSEs of $\hat{\phi}_1$ when SNR = 40 dB, as a function of the v.

1) Simulations Performed Varying The Few-cycles Signal

The estimator's behavior in few-cycles signals is crucial for DFT-based PMU methods, which rely on estimating and subtracting the interfering tone. This is particularly true when the length of the observation window (i.e., v) is between 3/5 and 5/2 cycles. Consequently, simulations were conducted, in the case of SNR = 40 dB, to assess the accuracy of the methods when v range from 0.6 to 4 cycles with a 0.01 cycles step.

Besides, the variances of the estimator $\hat{A}_1$ and $\hat{\phi}_1$ can attain the related unbiased CRLBs, which can be expressed as [29]:

$$\begin{cases} \left(\sigma_{\hat{A}_1}^2\right)_{CRLB} \cong \dfrac{2\sigma^2}{N} \\ \left(\sigma_{\hat{\phi}_1}^2\right)_{CRLB} \cong \dfrac{1}{N \cdot SNR} \end{cases} . \tag{23}$$

Fig. 5 and Fig. 6 show the MSEs for the estimated amplitude $\hat{A}_1$ and phase $\hat{\phi}_1$ as a function of the adopted v. As it can be observed, the proposed estimator (i) outperforms other methods (except the PSF-IpDFTc) when v < 0.8 cycles; (ii) has the same behavior as the e-IpDFT in the case of v > 0.8 cycles; (iii) does not need iterations while the e-IpDFT needs 2 or 3 iterations even if the frequency (i.e., v) is known. Moreover, the PSF-IpDFTc offers the best behavior because it uses linear sine-fit (LSF) to optimize the noise robustness of the IpDFTc. However, whether it is suitable for PMU measurements needs further study because the LSF may fail when the OOBI exists. In addition, the behavior of the proposed method is not affected by the adopted cycles v (also known as normalized frequency).
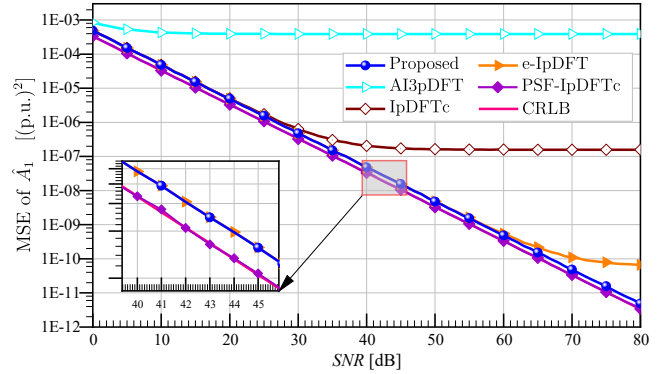

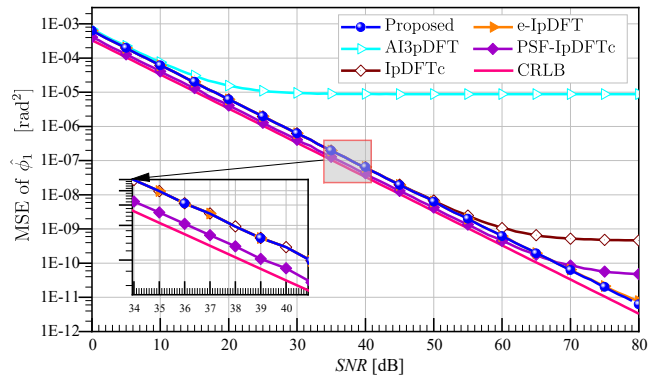Fig. 7. MSEs of $\hat{A}_1$ when v = 0.9 cycles, as a function of the SNR.

Fig. 8. MSEs of $\hat{\phi}_1$ when v = 0.9 cycles, as a function of the SNR.

2) Simulations Performed Varying The Noise Levels

To analyze the robustness of the proposed amplitude and phase estimator, estimation errors were investigated under different noise levels. The test signal is a sinewave with a window length of 0.9 cycles on which a Gaussian white noise with zero means has been superimposed. The noise levels range from 0 to 80 dB with 1 dB steps.

Fig. 7 and Fig. 8 show the MSEs for the estimated amplitude $\hat{A}_1$ and phase $\hat{\phi}_1$ as a function of the superposed noise level. As it can be observed, the proposed method (i) has the same behavior of the e-IpDFT in the case of *SNR* < 60 dB; (ii) has lower MSEs than the e-IpDFT in the case of *SNR* > 60 dB; (iii) outperforms PSF-IpDFTc when *SNR* > 70 dB. Therefore, the proposed estimator can be competitive with state-of-the-art methods under noisy conditions.

From the previous results, the behavior of the proposed estimator is independent of the adopted signal length and slightly dependent on the noise levels. This reveals that its systematic error is extremely small. In fact, the systematic error results from only the approximate expression (4) if the frequency of the estimated sinewave is known. This is because the proposed estimator utilizes both the positive and negative parts to estimate the amplitude and the phase. As such, the effects caused by spectrum leakage can be ignored in the estimation processes. These features, in addition to the frequency estimator FreqEst2, are another added value for the FiIpDFT's implementation in phasor estimation.

B. Performance of The FiIpDFT Phasor Estimator

To thoroughly evaluate the FiIpDFT method, all the static and dynamic tests were carried out according to the IEEE Stds [3-5]. For each test, the estimation accuracy is compared (i) with the most stringent requirements (P and M-class PMU); (ii) with the state-of-the-art method (i.e., the i-IpDFT method). The i-IpDFT is selected as comparison since it is not only the footstone of the FiIpDFT, but also one of the most outstanding PMU estimation methods. The sampling frequency is f_s = 50 kHz while the nominal frequency of the test signal is f_n = 50 Hz. The reporting rate (RR) is set to 50 frames/s unless otherwise specified. The initial phase of the test signals is a random value in the range of [0, 2π]. The window length is set to 60 ms, corresponding to three nominal cycles of the nominal system frequency (i.e., 3000 samples). For each test, the overall length of the analyzed signal is 250-nominal cycles. The reported results are the maximum TVE, FE, and RFE. These are the estimates computed repeatedly by shifting the window of 20 ms steps (i.e., 1000 samples). To approximate a more realistic operating scenario, Gaussian white noise with a 72 dB SNR, i.e., corresponding to a 12-bit analog-to-digital converter, is superimposed on the test signal. Other parameters, used for the i-IpDFT and FiIpDFT, are listed in Table II and are applied unless otherwise indicated. Note that the parameters of the i-IpDFT are selected as those reported in [17].

1) Frequency Deviation Test

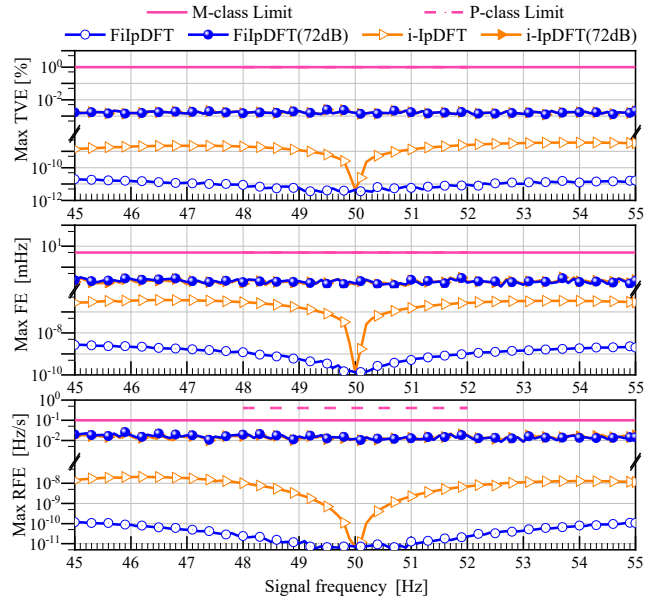The first static test is to assess the estimator's performance under frequency deviation conditions. The fundamental

Fig. 9. Maximum TVEs, FEs, and RFEs for the signal frequency test.

TABLE II OTHER PARAMETERS FOR I-IPDFT AND FIIPDFT

	P	Q	ξ	K	λ	Window
i-IpDFT	3	28	-	11	$3.3 \cdot 10^{-3}$	Hanning
FiIpDFT	-	18	$1 \cdot 10^{-7}$	11	$3.3 \cdot 10^{-3}$	Hanning

frequency f_1 of the test signal varies from 45 Hz to 55 Hz with an increment of 0.1 Hz. In this test, the limits of TVE and FE for both M- and P-class PMU are 1 % and 5 mHz. The limit of RFE for M- and P-class PMU are 0.1 and 0.4 Hz/s, respectively.

As reported in Fig. 9, the FiIpDFT has almost the same behavior as the i-IpDFT under 72 dB noise conditions. In the worst case, FiIpDFT's TVE, FE, and RFE do not exceed 0.0243 %, 0.333 mHz, and 0.025 Hz/s, respectively. Such errors are far less than the limits defined by the IEEE Std. For noise-free conditions, results demonstrate that the accuracy of FiIpDFT is almost unaffected by the frequency deviation. This is due to the more robust technique adopted in the FiIpDFT compared to the i-IpDFT.

2) Harmonic Distortion Test

The second static test evaluates the estimator's behavior under harmonic interference conditions. In this test, the test signal contains a fundamental component plus a single harmonic component whose amplitude is A_h, and the harmonic order varies from 2 to 50. For the P- and M-class tests, A_h is set to 1 % and 10 % of A_1, respectively. Considering a more realistic operating scenario, f_1 is set to 50.5 Hz to avoid synchronous sampling. Under these conditions, TVE limit is 1 % for both P- and M-class PMU, while FE limits are 25 and 5 mHz, respectively. Moreover, the limit of RFE is regarded as 0.4 Hz/s only for the P-class PMU.

Fig. 10 and Fig. 11 demonstrate that the FiIpDFT has similar behavior as the i-IpDFT when *SNR* = 72 dB, with either 1 % or 10 % harmonic distortion level. As for the noise-free test results, the farther from the fundamental, the smaller the influence of harmonics on the estimation accuracy. For the 10 % harmonic
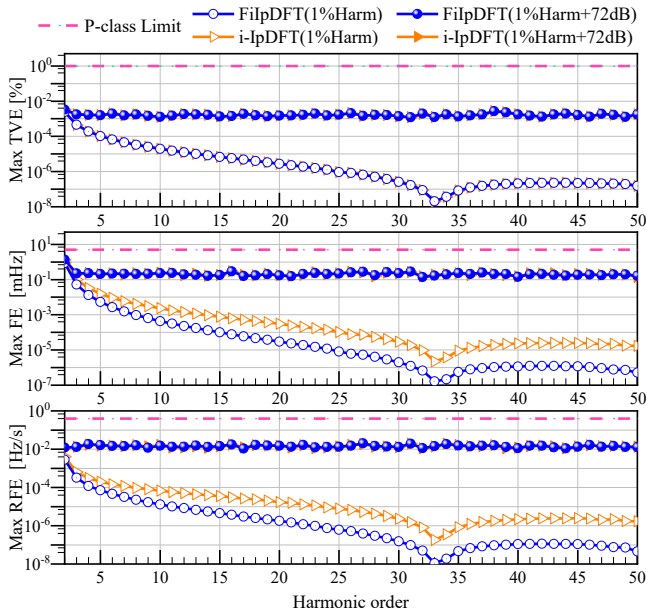
Fig. 10. Maximum TVEs, FEs, and RFEs in the presence of 1 % harmonics.

Fig. 12. Maximum TVEs, FEs, and RFEs for the OOBI test ($10 \le f_i \le 25$ Hz).

distortion test (i.e., M-class test), the worst-case result (i.e., maximum TVE and FE are 0.0033 % and 0.4618 mHz) is obtained in the presence of the 4th harmonic rather than the 2nd or 3rd harmonic. This is because the iterative routine is activated under the 2nd or 3rd harmonic conditions when K is set to 11. Differently from the 10 % harmonic tests, the iterative routine is not activated in the 1 % harmonic distortion test (i.e., P-class tests). So, the worst-case result is obtained in the presence of the 1 % 2nd harmonic (i.e., maximum TVE and FE are 0.0036 % and 1.431 mHz). As regards RFE, the IEEE Std [5] does not define a limit for M-class tests, but the maximum RFE of the FiIpDFT is 0.0257 Hz/s, which is far less than 0.4 Hz/s.

3) OOBI Tests

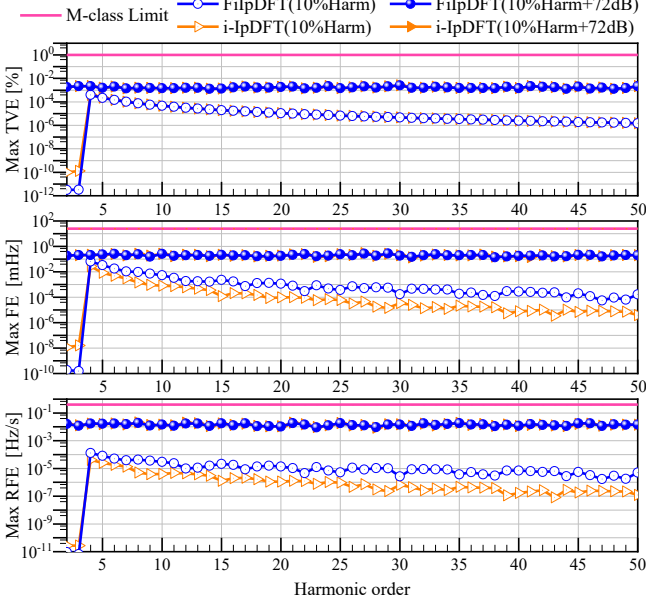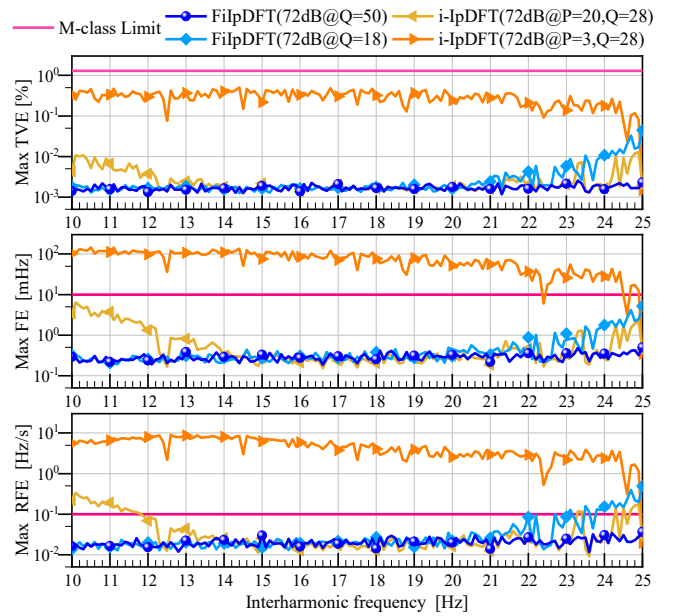In the third static test, the robustness of the proposed FiIpDFT method is evaluated under sub- and inter-harmonic

interference conditions. For this analysis, f_1 is set to 47.5 and 52.5 Hz for sub- and inter-harmonic tests, respectively. The A_i, amplitude of the sub- or inter-harmonic component, is 10 % of the fundamental. f_i, the frequency of sub- or inter-harmonic, varies within 10 and 25 or 75 or 100 Hz with an increment of 0.1 Hz. In this test, the latest IEEE Std [5] fixes the limits of TVE and FE for M-class PMU at 1.3 % and 10 mHz. There is no requirement for RFE for OOBI test in [5], but the limit of RFE is 0.1 Hz/s for assessing the behavior of estimators.

Additionally, two different parameter configurations are used for both methods to help us understand the estimator's behavior comprehensively. For the i-IpDFT, $P = 3$, $Q = 28$ is set as reported in [17], $P = 20$, $Q = 28$ is set to let the i-IpDFT meet the baseline limits of the IEEE in the OOBI test ($f_1 = 47.5$ Hz, 10 Hz $\le f_i \le 25$ Hz). For the FiIpDFT, $Q = 18$ is used to meet the baseline limits and $Q = 50$ is used to show that the

Fig. 11. Maximum TVEs, FEs, and RFEs in the presence of 10 % harmonics.
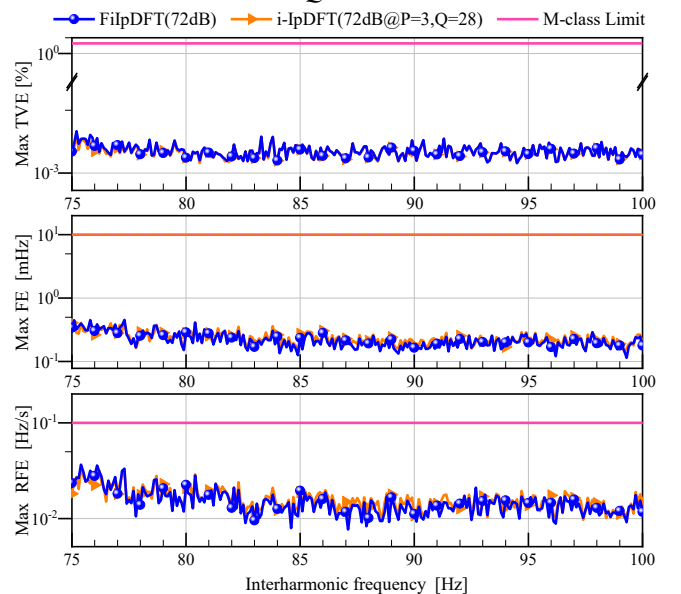
Fig. 13. Maximum TVEs, FEs, and RFEs for the OOBI test ($75 \le f_i \le 100$ Hz).

FiIpDFT can provide better behavior without any severe increase in computing burden.

All test results are reported in Fig. 12 and Fig. 13. The significant difference between the two methods appears when $10 \le f_i \le 25$ Hz (Fig. 12). The FiIpDFT, when $Q = 18$, satisfies the requirements with maximum TVE, FE, and RFE of 0.044 %, 5.225 mHz, and 0.493 Hz/s, respectively. While when $Q = 50$, it achieves higher accuracy with maximum TVE, FE, and RFE of $2.7 \cdot 10^{-3}$ %, 0.500 mHz, and 0.037 Hz/s, respectively. All metrics of the FiIpDFT well fulfill the IEEE Std under 72 dB noise conditions. However, the i-IpDFT does not satisfy the requirements when $P = 3$, $Q = 28$. Actually, P iterations are used to compensates the effects of the negative image of the fundamental tone and Q iterations are used to compensate the effects of a generic interfering tone [17]. Hence, the estimation error of the i-IpDFT can be reduced by increasing the number of iterations P and Q. Since the AI3pDFT [23] and the e-IpDFT [16] are not performing well within the frequency band of 10 Hz to 15 Hz (i.e., corresponding to the first DFT bin), more iterations P are needed to satisfy the requirements. So, the i-IpDFT satisfies the requirements only when $P = 20$, $Q = 28$.

In each estimate, the FiIpDFT requires no more than 18 iterations to meet the requirements (18 iterations in the worst-case scenario), while the i-IpDFT requires 1197 iterations. Such a significant improvement in computing efficiency is based on two main reasons. First, the proposed RI3pDFT does not require any iteration to eliminate the effects of negative image interference. Second, the RI3pDFT used in the FiIpDFT is more accurate than that of the e-IpDFT used in the i-IpDFT under frequency deviation or short window conditions (i.e., when f_i is between 10 Hz and 15 Hz). Third, the two-stop criterion used in the FiIpDFT avoids a lot of redundant iterations. This allows the FiIpDFT to use fewer iterations to compensate for the effect of interfering tones, as compared with the i-IpDFT.

4) Frequency Ramp Tests

In the first dynamic test, the proposed estimator's behavior is evaluated under fundamental frequency ramp conditions. This test is used to simulate the imbalance scenario between the load and the generation in the power system. For this specific test, f_1 varies between 45 and 55 Hz with a rate of change of 1 Hz/s. The TVE, FE, and RFE are reported as a function of ramp frequency. The IEEE Std specifies that (i) the limits of TVE and FE, for both M- and P-class PMU, are 1 % and 10 mHz; (ii) the limits of RFE for M- and P-class PMU are 0.2 and 0.4 Hz/s, respectively. As reported in Fig. 14, the FiIpDFT performs in this part with maximum TVE, FE, and RFE of $3.8 \cdot 10^{-2}$ %, 0.2485 mHz, and $1.77 \cdot 10^{-2}$ Hz/s, respectively. Clearly, the proposed FiIpDFT method fully satisfies both P- and M-class requirements and achieves the same orders of magnitude accuracy on phasor estimation compared to state-of-the-art i-IpDFT method.

5) Modulation Tests

The second dynamic test is performed to evaluate the behavior of the FiIpDFT method under small oscillations. In detail, it assesses the estimation accuracy in the presence of amplitude or phase-modulated conditions. The general model of the modulated signal is:
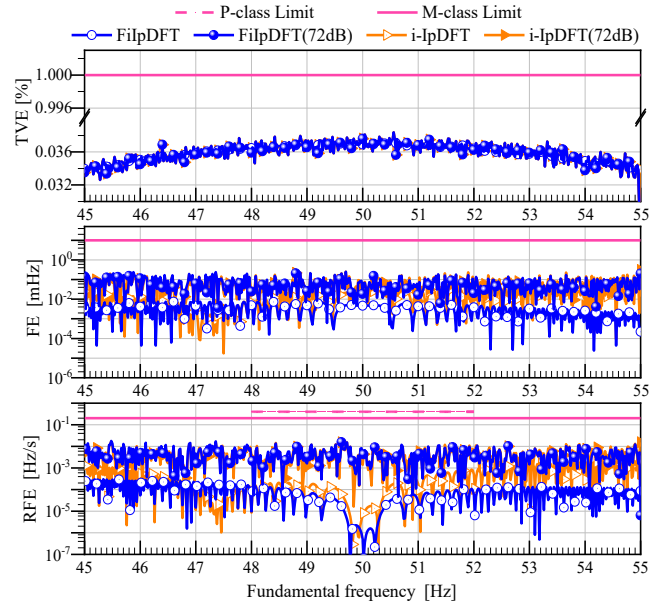
Fig. 14. TVEs, FEs, and RFEs for the frequency ramp test.

$$x(n) = \sqrt{2}X\left(1 + x_m(n)\right)\cos\left(\phi_m(n)\right), \tag{24}$$

where X is the common rms magnitude and:

$$\begin{aligned} x_m(n) &= k_a \cos\left(2\pi f_m n T_s\right) \\ \phi_m(n) &= 2\pi f_1 n T_s + k_p \cos\left(2\pi f_m n T_s - \pi\right) \end{aligned}, \tag{25}$$

where k_a and k_p represent the modulation depths of amplitude and phase, respectively. f_m is the modulation frequency, which varies from 0.1 Hz to 5 Hz with 0.1 Hz steps. The worst case defined in [5] has been considered, i.e., $k_a = 0.1$, $k_p = 0$ rad during amplitude modulation tests and $k_a = 0$, $k_p = 0.1$ rad under the phase modulation conditions. In this context, the IEEE Std limit of TVE for both M- and P-class PMU is 3 %. The limits of FE for M- and P-class PMU are 300 mHz and 60 mHz, respectively. The limits of RFE for M- and P-class PMU are 14 and 2.3 Hz/s, respectively.

Fig. 15. Maximum TVEs, FEs, and RFEs for the amplitude modulation test.

Fig. 16. Maximum TVEs, FEs, and RFEs for the phase modulation test.
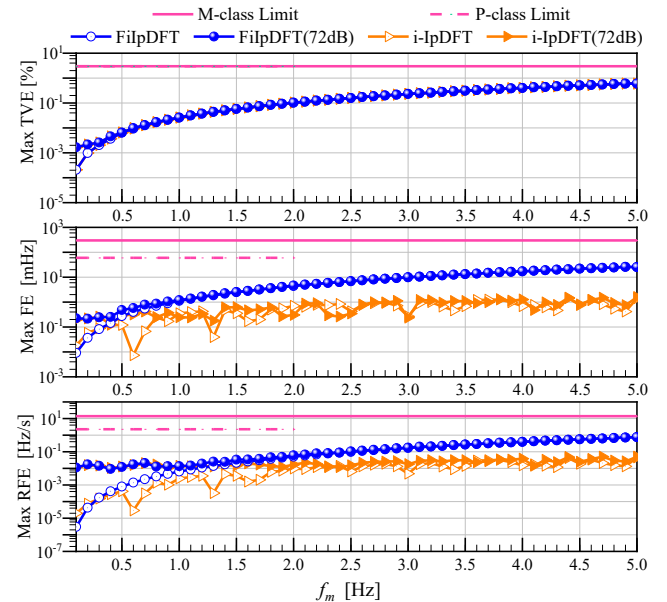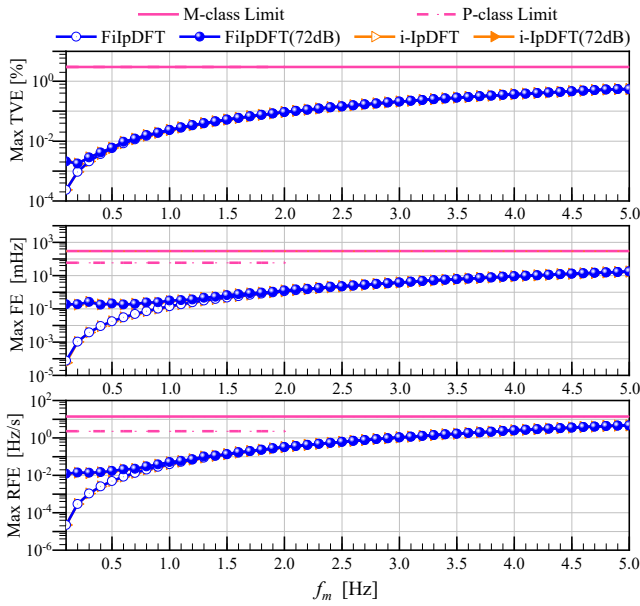
Fig. 15 and Fig. 16 illustrate the results obtained from amplitude and phase modulation tests. It is observed that the FiIpDFT satisfy both P- and M-class requirements. In both the amplitude and phase modulation tests, the estimation error increases with the increase of the modulation frequency, and noise is no longer the main factor when the modulation frequency $f_m > 1$Hz. The worst-case performance of the estimators is obtained at $f_m = 5$ Hz. In the amplitude modulation test, the maximum TVE, FE, and RFE of the FiIpDFT are 0.599 %, 25.63 mHz, and 0.759 Hz/s, respectively. In the phase modulation test, the maximum TVE, FE, and RFE of the FiIpDFT are 0.547 %, 17.77 mHz, and 4.624 Hz/s, respectively.

Test results reported in Fig. 16 demonstrate that the FiIpDFT has the same behavior compared with the i-IpDFT under phase modulation test. In the case of amplitude modulation, the maximum TVE curves associated with the FiIpDFT and the i-IpDFT overlap (see Fig. 15). However, the frequency estimation accuracy of the FiIpDFT is lower than the i-IpDFT in the presence of amplitude modulation. This is due to the FreqEst1 performing better than the FreqEst2 used in the FiIpDFT in such situation, which leads to the e-IpDFT [16] outperforming the proposed RI3pDFT. Fortunately, the proposed amplitude estimator is robust enough to result in the same accuracy of the phasor as the i-IpDFT in this context. Anyway, the maximum FE (25.63 mHz) of the FiIpDFT is far less than limit (300 mHz).

6) Amplitude and Phase Step Tests

To assess the estimator's responsiveness to a transient event, the third dynamic test is conducted during an instantaneous step change, i.e., amplitude (10 %) and phase ($\pi/18$) step tests. In these tests, M-class PMUs require that the response time of phasor, frequency, and ROCOF estimations should not exceed 140, 280, and 280 ms, respectively. P-class PMUs require the response time of phasor, frequency, and ROCOF estimations should not exceed 40, 90, and 120 ms, respectively. Both P- and M-class PMUs require that the delay time should not exceed 5

ms. The maximum overshot for the M- and P-class PMU should not exceed 10 % or 5 % of step magnitude. For the sake of simplicity, only positive step tests are reported in this article. This analysis is performed in two situations: first, at the RR = f_s frames/s under noise-free condition; second, at the RR = 50 frames/s under 72 dB noise condition. To avoid synchronous sampling f_1 is set to 51 Hz.

Fig. 17. TVEs, FEs, and RFEs under the step change in amplitude.
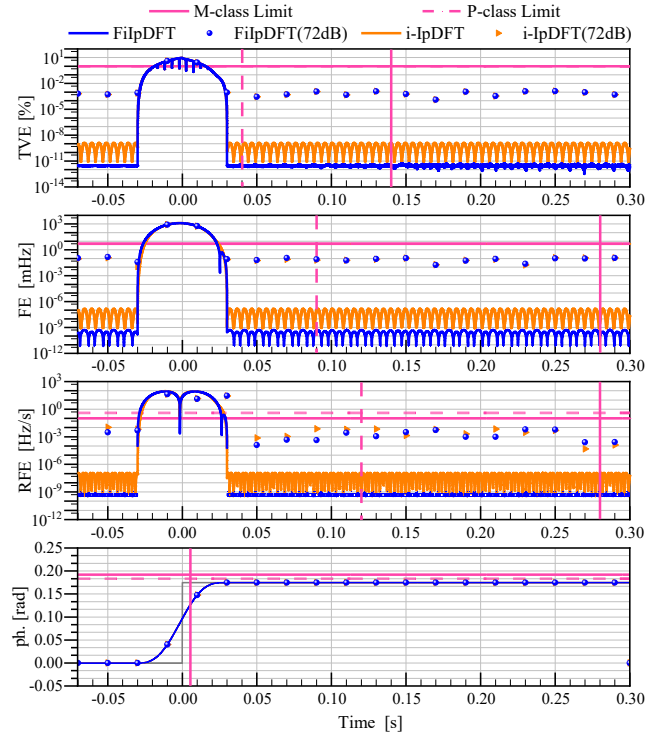
Fig. 18. TVEs, FEs, and RFEs under the step change in phase.

Fig. 17 and Fig. 18 show the estimated amplitude (A) and phase (ph) over time. Moreover, the TVE, FE, and RFE are all represented as a function of time. It is observed that the FiIpDFT for amplitude and phase step tests comply with the IEEE Std. The results under noise-free conditions are summarized first. In the amplitude step test, the response times of the TVE, FE, and RFE are 28.12, 49.96, and 58.28 ms, respectively. In the phase step test, the response times of the TVE, FE, and RFE are 34.08, 49.54, and 55.54 ms, respectively. The delay times in both the amplitude and phase step tests are 2.86 and 1.56 ms, respectively. The overshot in both the amplitude and phase step tests is zero. In the case of the RR = 50 frames/s and 72 dB noise, the TVE and FE follow the same trend as in the presence of noise-free condition. Although the response time of REF does not remain consistent with results obtained from noise-free condition (especially in phase step test), it is still far below the limit required by P-class requirements.

C. Computational Complexity

To evaluate the practicality of implementing the FiIpDFT method into an embedded hardware solution, its computational complexity is analysed. This is not achieved only theoretically, but also by means of simulations in MATLAB. The number of arithmetic operations for each step are listed in Table III, along with the total number of arithmetic operations. The average execution times of the estimators during each test are reported in Table IV.

1) Theoretical Analysis

The FiIpDFT's computational burden comes mainly from two aspects: the RI3pDFT and the iterative routine. The RI3pDFT used in the FiIpDFT requires 39 simple and 10 complex operations while the AI3pDFT used in the e-IpDFT requires 20 simple and 6 complex operations [23, 25]. However, the e-IpDFT used in the i-IpDFT needs to be iterated P ($P \geq 2$) times to eliminate interference of the negative image (i.e., e-IpDFT reported in [16] and [17]). This reveals that the RI3pDFT used in the FiIpDFT is faster than the e-IpDFT.

The second source of computational burden is the iterative routine. Firstly, a simplified formula (4) is introduced to compute the DTFT of the Hanning window. This allows the FiIpDFT require only 7 simple and 3 complex operations for each DTFT calculation, while the i-IpDFT needs 37 simple and 24 complex operations [17, 25]. In addition, since two-stop criterion is used in the FiIpDFT, its computation burden depends on the frequency, amplitude, and phase of the interfering tone. Considering the worst scenario, the FiIpDFT ($K = 11$ and the maximum iteration number $Q = 50$) requires 8835 simple and 2193 complex operations, while the i-IpDFT ($K = 8$ $P = 2$, and $Q = 28$) requires 62023 simple and 40641 complex operations [25]. In fact, FiIpDFT's iteration number is always less than Q in most cases. It is, thus, reasonable to say that the FiIpDFT is theoretically much faster than the i-IpDFT in the presence of the OOBI.

2) Simulation Analysis

The computational efficiency of the FiIpDFT was also analysed using simulations, and the results are reported in Table

IV. All tests are conducted by MATLAB R2019b running on a computer with 16-GB RAM and a 2.3-GHz processor. In each case, the input signal is the same as the corresponding test signal in section IV.B. Input signals with an overall length of 100 seconds, meaning 4997 runs when RR = 50 frame/s, are used to obtain the average execution time of all estimates. The average number of calls to the RI3pDFT/AI3pDFT used in the FiIpDFT/i-IpDFT has also been reported. Parameters used for the i-IpDFT and FiIpDFT are the same as for Section IV-B unless otherwise indicated in Table IV. In each estimate, the FiIpDFT requires no more than $2 \cdot Q + 1$ calls of the RI3pDFT. While the i-IpDFT requires $2 \cdot Q + 1$ calls of the e-IpDFT, i.e., $(2 \cdot Q + 1) \cdot (P + 1)$ calls of the AI3pDFT. The shadowed cells correspond to the results that are not compliant with the requirements of the IEEE std. The bolded cells represent the best behavior under the same test conditions.

For non-OOBI tests (i.e., Sign Freq, 1 % 2nd Harm Dist, Ampl Mod, Ph Mod, and Freq Ramp), both the FiIpDFT and the i-IpDFT do not need to eliminate OOBI by iteration. In these cases, the FiIpDFT's iterative routine will not be activated, while the i-IpDFT requires 4 calls of the AI3pDFT to eliminate the effects of the negative image. Although the computational efficiency of the proposed RI3pDFT is not as good as the AI3pDFT, it is lighter than that of the e-IpDFT because the e-IpDFT requires $P + 1$ calls of the AI3pDFT. Consequently, the computational efficiency of the FiIpDFT is about 1.8 times that of the i-IpDFT when $P = 3$ is used for the i-IpDFT.

For the 10 % 2nd harmonic tests, the computational efficiency of the FiIpDFT is about 19 times that of the i-IpDFT. This is because the i-IpDFT needs to run the AI3pDFT 228 times in each estimate, while the FiIpDFT only runs the RI3pDFT 8.21 times on average. If the FiIpDFT does not use the second stop criterion $\nabla \hat{f}_1^q$, it needs to run the RI3pDFT 37 times in each estimate when $Q = 18$. This means the second stop criterion $\nabla \hat{f}_1^q$ increases the computational efficiency of the FiIpDFT by a factor of 4.5 in the 10 % 2nd harmonic situations.

For the $f_1 = 52.5$ Hz OOBI tests, the computational efficiency

TABLE III FiIpDFT COMPUTATIONAL COMPLEXITY

		Parameter	Value
		K	11
		Q	≤ 50
	$+ \mid - \mid \times$	$\div \mid exp \mid sin \mid sqrt$	funct
(A) $W_H(\cdot)$	7	3	-
(B) RI3pDFT	-	-	(B1) + (B2)
(B1) Freq	6	2	-
(B2) Phasor	33	8	-
FiIpDFT	$+ \mid - \mid \times$	$\div \mid exp \mid sin \mid sqrt$	function
line 2	-	-	(B)
line 3	$5K$	-	$K \cdot$(A)
line 4	$5K - 2$	-	-
line 6, 8	K	-	$Q \cdot$(B)
line 7, 9	$Q \cdot 5K$	-	$Q \cdot K \cdot$(A)
line 10	Q	-	-
Total	$172 \cdot Q + 235$	$43 \cdot Q + 43$	-

TABLE IV THE AVERAGE EXECUTION TIMES OF THE ESTIMATORS

Cases	Methods	TVE_{max} [%]	FE_{max} [mHz]	RFE_{max} [Hz/s]	Time [ms]	Calls[5]
Sign Freq	i-IpDFT	0.0029	0.3478	0.0264	0.2232	4
	FIlpDFT	0.0029	0.3759	0.0271	**0.1233**	**1**
Harm Dist (10% 2nd)	i-IpDFT[1]	0.0019	0.2180	0.0163	7.8961	228
	FIlpDFT[3]	0.0019	0.2101	0.0161	**0.4048**	**8.21**
Harm Dist (1% 2nd)	i-IpDFT	0.0039	1.0505	0.0219	0.1854	4
	FIlpDFT	0.0039	1.4645	0.0236	**0.0984**	**1**
OOBI (f_i=47.5Hz)	i-IpDFT[1]	0.5056	143.4549	9.1947	7.1023	228
	i-IpDFT[2]	0.0125	5.5715	0.2927	31.696	1197
	FIlpDFT[3]	0.0624	7.3988	0.7145	**1.1284**	**28.9**
	FIlpDFT[4]	**0.0028**	**0.5412**	**0.0332**	1.2353	35.5
OOBI (f_i=52.5Hz)	i-IpDFT[1]	0.0029	0.4425	0.0357	7.3585	228
	FIlpDFT[4]	0.0028	0.4780	0.0329	**0.8246**	**23.6**
Ampl Mod	i-IpDFT	0.6039	**1.5881**	**0.0575**	0.2093	4
	FIlpDFT	0.6039	25.7483	0.7630	**0.1131**	**1**
Ph Mod	i-IpDFT	0.5477	17.510	4.6350	0.2230	4
	FIlpDFT	0.5477	17.788	4.6405	**0.1201**	**1**
Freq Ramp	i-IpDFT	0.0388	0.2565	0.0174	0.2940	4
	FIlpDFT	0.0388	0.3098	0.0183	**0.1660**	**1**

[1]The i-IpDFT adopts $P = 3$ and $Q = 28$ as iteration parameters. [2]The i-IpDFT adopts $P = 20$ and $Q = 28$ as iteration parameters. [3]The FIlpDFT adopts $Q = 18$ as iteration parameters. [4]The FIlpDFT adopts $Q = 50$ as iteration parameters. [5]The average calls of the RI3pDFT/AI3pDFT used in the FIlpDFT/i-IpDFT.

of the FIlpDFT is about 9 times that of the i-IpDFT. Different from the 10 % 2nd harmonic tests, the FIlpDFT requires more iterations due to the frequency the interfering tone is closer to the fundamental. The FIlpDFT requires to run the RI3pDFT 23.6 times on average. So, the stop criterion $\nabla \hat{f}_1^q$ increases the computational efficiency of the FIlpDFT by a factor of 4.3.

The improvement of the FIlpDFT becomes more notable when the $f_1 = 47.5$ Hz OOBI tests (the interference tone's frequency f_i is between 10 and 25 Hz). The average execution time of the FIlpDFT and the i-IpDFT is 1.1284 ms and 31.696 ms, respectively, to meet the requirements listed in the IEEE Std. The computational efficiency of the FIlpDFT is about 28 times that of the i-IpDFT. In this situation, the i-IpDFT requires to run the AI3pDFT 1197 times (corresponding to $P = 20$, $Q = 28$), and it cannot meet the requirements if $P < 20$. While the FIlpDFT requires to run the RI3pDFT only 28.9 (when $Q = 18$) or 35.5 (when $Q = 50$) times on average. This means the second stop criterion $\nabla \hat{f}_1^q$ increases the computational efficiency of the FIlpDFT by a factor of 1.28 or 2.85. Hence, it is not notable compared with the 10 % 2nd harmonic situations. In the $f_1 = 47.5$ Hz OOBI tests, however, the FIlpDFT significantly outperforms the i-IpDFT. The main reason is entirely due to the RI3pDFT used by the FIlpDFT outperforms the e-IpDFT or AI3pDFT used in the i-IpDFT under a short observation window condition (i.e., the f_i varies from 10 to 25 Hz corresponding to a window length varying from 3/5 to 3/2 cycles, when $f_s = 50$ kHz and 3000 samples are used.).

TABLE V RESULTS OF MULTIPLE INTERFERENCES

Signal	J [cycles]	TVE_{max} [%] FIlpDFT	TVE_{max} [%] i-IpDFT	FE_{max} [mHz] FIlpDFT	FE_{max} [mHz] i-IpDFT	RFE_{max} [Hz/s] FIlpDFT	RFE_{max} [Hz/s] i-IpDFT
a. f_1=47.5 OOBI(10Hz)+ Harmonics (2nd+3rd)	4	**0.1308**	0.3100	23.793	85.209	0.3874	4.0945
	5	0.0625	**0.0583**	**5.1100**	6.7817	0.1166	0.1684
	6	0.0340	**0.0323**	2.4176	**1.6369**	0.0411	**0.0355**
b. f_1=47.5 OOBI(25Hz)+ Harmonics (2nd+3rd)	4	**0.1710**	0.8229	37.498	373.97	0.9210	19.871
	5	**0.2547**	0.2548	76.358	99.973	7.4181	9.7210
	6	0.0331	**0.0295**	**1.9179**	2.0952	**0.0214**	0.0279
c. f_1=52.5 OOBI(75Hz)+ Harmonics (2nd+3rd)	4	**1.0971**	1.1048	377.74	461.58	15.539	14.441
	5	**0.2723**	0.2725	100.77	120.96	8.8336	11.959
	6	**0.0124**	0.0127	**0.6472**	0.9505	**0.0151**	0.0191
d. f_1=47.5 OOBI(10Hz)+ Harmonics+ (2nd+3rd) InterH(125Hz)	4	0.1649	**0.1505**	29.089	54.621	0.8118	2.2864
	5	**0.0715**	0.0718	5.5008	**4.7174**	0.1576	0.1825
	6	0.0337	**0.0323**	2.4299	**1.5938**	0.0418	**0.0406**
e. f_1=47.5 OOBI(25Hz)+ Harmonics+ (2nd+3rd) InterH(125Hz)	4	**0.6745**	0.8465	290.13	372.69	27.702	36.078
	5	**0.2343**	0.2399	76.879	99.910	7.5545	9.7993
	6	0.0342	**0.0305**	2.4759	**1.6665**	0.0437	**0.0309**
f. f_1=52.5 OOBI(75Hz)+ Harmonics+ (2nd+3rd) InterH(125Hz)	4	1.0571	**0.8280**	470.77	385.64	45.921	37.797
	5	0.3172	**0.1976**	119.13	98.972	4.7413	5.3784
	6	**0.0125**	0.0128	0.8880	**0.6200**	0.0357	**0.0258**
Limit	-	1.3	1.3	10	10	0.1	0.1

TABLE VI TOTAL EXECUTION TIME (FOR 50 S SIGNAL) UNDER MULTIPLE INTERFERENCES WHEN 6 CYCLES OBSERVATION WINDOW IS CONSIDERED[1]

	a. [s]	b. [s]	c. [s]	d. [s]	e. [s]	f. [s]
i-IpDFT	15.920	16.499	15.890	16.186	14.719	17.254
FIlpDFT	**1.1210**	**1.0860**	**1.1030**	**1.0950**	**0.9700**	**1.1960**

[1]The processing signals with a length of 50 seconds correspond to 2494 estimates when the time window is 120 ms (i.e., 6 cycles) and RR = 50 frame/s.

D. Limitations of the FIlpDFT: Multiple Interferences

Multiple interferences may occur in practicality, even though IEEE Stds do not provide any guidelines for this. Considering the FIlpDFT's signal model (19), the same as the i-IpDFT, contains only one interference tone, it is significant to analyze the behavior of the FIlpDFT against multiple interferences. To this end, following test signals are considered:

a) signal with $f_1 = 47.5$ Hz simultaneously distorted by 10 % interharmonic ($f_i = 10$ Hz), 10 % 2nd and 10 % 3rd harmonics;

b) signal with $f_1 = 47.5$ Hz simultaneously distorted by 10 % interharmonic ($f_i = 25$ Hz), 10 % 2nd and 10 % 3rd harmonics;

c) signal with $f_1 = 52.5$ Hz simultaneously distorted by 10 % interharmonic ($f_i = 75$ Hz), 10 % 2nd and 10 % 3rd harmonics.

In addition, the signals of cases *d)*, *e)*, and *f)* are the signals in *a)*, *b)*, and *c)* superimposed with another 10% interharmonic (i.e., 125 Hz) between the 2nd and 3rd harmonics, respectively.

In fact, both FIlpDFT and i-IpDFT cannot work well on these test signals when 3 cycles of data samples are used. Thus, the window length $J = 4$, 5, and 6 cycles are considered in this test. The length of the overall test signal is 50 seconds. Other setups are the same as are described in Section IV-B.

The maximum TVEs, FEs, and RFEs are listed in Table V. Since the requirements of these tests are not specified in IEEE Stds, the behavior of the FIlpDFT is only compared with the

limits of OOBI tests in Standard [4]. The results show that both methods satisfy the requirements only when the 6 cycles observation window is used. The FiIpDFT cannot deal with these three test signals when the time window is less than 6 cycles due to two reasons. First, there are three/four strong and nearby interferences, which produce short and long-range spectral leakage simultaneously, are a serious challenge for all IpDFT-based methods. Second, the limitations of the FiIpDFT signal model. As the signal model (19) contains only one interference, it is hard to eliminate all three or four interferences even if the number of iterations becomes larger.

Both methods have advantages and disadvantages compared to each other under multiple interference situations. However, the FiIpDFT's computational efficiency is at least 14 times that of the i-IpDFT as reported in table VI. The FiIpDFT provides sufficient accuracy in all these tests when the observation length is 120 ms, which is less than the latency limit of M-class PMU (i.e., 140 ms). When multiple interferences are present, however, the FiIpDFT requires a longer observation window than the TWLSMP [12] and the PCA-MPM [30] methods to eliminate the contributions of the OOBIs.

V. CONCLUSION

In this work, a IpDFT-based phasor estimation method, i.e., FiIpDFT, has been presented. The contribution is threefold: firstly, a novel and robust amplitude and phase estimator has been proposed to accurately estimate amplitude and phase without iteration in the presence of frequency deviation. Secondly, a straightforward formula, used to reconstruct the DFT spectrum, has been introduced to lower the computational complexity in each iteration. Additionally, two-stop criterion have been proposed to avoid the periodicity redundant iterations of the OOBI elimination process. The performance of the FiIpDFT is evaluated against requirements for both P- and M-class PMUs defined in the latest IEEE Std, and results indicated that the FiIpDFT, using a three cycles observation window, meets all the requirements. Moreover, the FiIpDFT achieves the same estimation accuracy as the i-IpDFT except for the amplitude modulation test. Finally, the FiIpDFT's computational efficiency is at least 8 times that of the i-IpDFT in the OOBI tests, and is 1.8 times that in other tests.

REFERENCES

[1] X. Guo, S. Lou, Y. Wu, and Y. Wang, "Low-Carbon Operation of Combined Heat and Power Integrated Plants Based on Solar-Assisted Carbon Capture," *J Mod Power Syst Cle*, pp. 1-13, 2021.
[2] A. Monti, C. Muscas, and F. Ponci, *Phasor Measurement Units and Wide Area Monitoring Systems: From the Sensors to the System*, New York, NY, USA: Elsevier Academic Press, 2016.
[3] I. S. ASSOCIATION, "IEEE Standard for Synchrophasor Measurements for Power Systems -- Amendment 1: Modification of Selected Performance Requirements," *IEEE Std C37.118.1a-2014 (Amendment to IEEE Std C37.118.1-2011)*, pp. 1-25, 2014.
[4] I. S. ASSOCIATION, "IEEE Standard for Synchrophasor Measurements for Power Systems," *IEEE Std C37.118.1-2011 (Revision of IEEE Std C37.118-2005)*, pp. 1-61, 2011.
[5] IEC/IEEE, "IEEE/IEC International Standard - Measuring relays and protection equipment - Part 118-1: Synchrophasor for power systems - Measurements," *IEC/IEEE 60255-118-1:2018*, pp. 1-78, 2018.
[6] J. A. D. L. O. Serna, "Dynamic phasor estimates for power system oscillations," *IEEE T Instrum Meas,* vol. 56, no. 5, pp. 1648-1657, Oct, 2007.
[7] M. A. Platas-Garza, and J. A. D. Serna, "Dynamic Phasor and Frequency Estimates Through Maximally Flat Differentiators," *IEEE T Instrum Meas,* vol. 59, no. 7, pp. 1803-1811, Jul, 2010.
[8] D. Belega, D. Fontanelli, and D. Petri, "Dynamic Phasor and Frequency Measurements by an Improved Taylor Weighted Least Squares Algorithm," *IEEE T Instrum Meas,* vol. 64, no. 8, pp. 2165-2178, Aug, 2015.
[9] D. Belega, D. Fontanelli, and D. Petri, "Low-Complexity Least-Squares Dynamic Synchrophasor Estimation Based on the Discrete Fourier Transform," *IEEE T Instrum Meas,* vol. 64, no. 12, pp. 3284-3296, Dec, 2015.
[10] M. Bertocco, G. Frigo, C. Narduzzi, C. Muscas, and P. A. Pegoraro, "Compressive Sensing of a Taylor-Fourier Multifrequency Model for Synchrophasor Estimation," *IEEE T Instrum Meas,* vol. 64, no. 12, pp. 3274-3283, Dec, 2015.
[11] R. Ferrero, P. A. Pegoraro, and S. Toscani, "Synchrophasor Estimation for Three-Phase Systems Based on Taylor Extended Kalman Filtering," *IEEE T Instrum Meas,* vol. 69, no. 9, pp. 6723-6730, Sept, 2020.
[12] J. Song, J. Zhang, and H. Wen, "Accurate Dynamic Phasor Estimation by Matrix Pencil and Taylor Weighted Least Squares Method," *IEEE T Instrum Meas,* vol. 70, pp. 1-11, 2021.
[13] P. Tosato, D. Macii, M. Luiso, D. Brunelli, D. Gallo, and C. Landi, "A Tuned Lightweight Estimation Algorithm for Low-Cost Phasor Measurement Units," *IEEE T Instrum Meas,* vol. 67, no. 5, pp. 1047-1057, May, 2018.
[14] C. Narduzzi, M. Bertocco, G. Frigo, and G. Giorgi, "Fast-TFM-Multifrequency Phasor Measurement for Distribution Networks," *IEEE T Instrum Meas,* vol. 67, no. 8, pp. 1825-1835, Aug, 2018.
[15] D. Macii, D. Petri, and A. Zorat, "Accuracy Analysis and Enhancement of DFT-Based Synchrophasor Estimators in Off-Nominal Conditions," *IEEE T Instrum Meas,* vol. 61, no. 10, pp. 2653-2664, Oct, 2012.
[16] P. Romano, and M. Paolone, "Enhanced Interpolated-DFT for Synchrophasor Estimation in FPGAs: Theory, Implementation, and Validation of a PMU Prototype," *IEEE T Instrum Meas,* vol. 63, no. 12, pp. 2824-2836, Dec, 2014.
[17] A. Derviskadic, P. Romano, and M. Paolone, "Iterative-Interpolated DFT for Synchrophasor Estimation: A Single Algorithm for P- and M-Class Compliant PMUs," *IEEE T Instrum Meas,* vol. 67, no. 3, pp. 547-558, Mar, 2018.
[18] H. J. Nussbaumer, "The fast Fourier transform," *Fast Fourier Transform and Convolution Algorithms*, pp. 80-111: Springer, 1981.
[19] D. Belega, and D. Dallet, "Multifrequency signal analysis by Interpolated DFT method with maximum sidelobe decay windows," *Measurement,* vol. 42, no. 3, pp. 420-426, Apr, 2009.
[20] D. Belega, and D. Petri, "Effect of noise and harmonics on sine-wave frequency estimation by interpolated DFT algorithms based on few observed cycles," *Signal Processing,* vol. 140, pp. 207-218, 2017.
[21] C. Li, J. Zhang, and H. Wen, "Accurate and Fast Amplitude Estimation of Signal Distorted by Noise and Harmonics for Control of VSI," *IEEE T Ind Electron,* vol. 68, no. 12, pp. 12584-12594, 2021.
[22] T. Jin, and W. Zhang, "A Novel Interpolated DFT Synchrophasor Estimation Algorithm With an Optimized Combined Cosine Self-Convolution Window," *IEEE T Instrum Meas,* vol. 70, pp. 1-10, 2021.
[23] D. Agrez, "Weighted multipoint interpolated DFT to improve amplitude estimation of multifrequency signal," *IEEE T Instrum Meas,* vol. 51, no. 2, pp. 287-292, Apr, 2002.
[24] J. Borkowski, J. Mroczka, A. Matusiak, and D. Kania, "Frequency Estimation in Interpolated Discrete Fourier Transform With Generalized Maximum Sidelobe Decay Windows for the Control of Power," *IEEE T Ind Inform,* vol. 17, no. 3, pp. 1614-1624, 2021.
[25] G. Frigo, A. Derviskadic, and M. Paolone, "Reduced Leakage Synchrophasor Estimation: Hilbert Transform Plus Interpolated DFT," *IEEE T Instrum Meas,* vol. 68, no. 10, pp. 3468-3483, Oct, 2019.
[26] D. Belega, and D. Petri, "Fast procedures for accurate parameter estimation of sine-waves affected by noise and harmonic distortion," *Digital Signal Processing,* vol. 114, 2021.
[27] D. Belega, D. Petri, and D. Dallet, "Impact of harmonics on the interpolated DFT frequency estimator," *Mechanical Systems and Signal Processing,* vol. 66-67, pp. 349-360, Jan, 2016.
[28] D. Belega, and D. Petri, "Accuracy of the Synchrophasor Estimator Returned by the Interpolated DFT Algorithm Under Off-Nominal

Frequency and Harmonic Conditions," in IEEE Int Works Appl, 2018, pp. 1-6.

[29] S. M. Kay, *Fundamentals of statistical signal processing: estimation theory*: Prentice-Hall, Inc., 1993.

[30] L. Bernard, S. Goondram, B. Bahrani, A. Pantelous, and R. Razzaghi, "Harmonic and Interharmonic Phasor Estimation using Matrix Pencil Method for Phasor Measurement Units," *IEEE Sens J*, pp. 1-1, 2020.

Jian Song (S'20) received the B.S. degree in automation from Hunan University of Technology, Zhuzhou, China, in 2013, and the M.S. degree in electrical engineering in 2019 from the College of Electrical and Information Engineering, Hunan University, Changsha, China, where he is currently pursuing the Ph.D. degree. He is also a Joint Doctoral Student with the University of Bologna, Bologna, Italy, from 2021.

His current research interests include digital signal processing, power system wide area monitoring and PMU algorithms.

Alessandro Mingotti (S'17) was born in Cento (FE), Italy in 1992. He received the B.S., M.S., and Ph.D. degrees in electrical engineering from the University of Bologna, Bologna, Italy, in 2014, 2016, and 2020, respectively.

He is a Senior Assistant Professor at the University of Bologna from 2021. His research interests include management and condition maintenance of distribution networks, development, modelling, and metrological characterization of instrument transformers. He is also working on several National and European funded Projects.

Junhao Zhang (S'17, M'20) was born in Henan, China, in 1986. He received the B.Sc. and Ph.D. degrees from Hunan University in 2009, and 2019, respectively. He is currently working as a Postdoc in the College of Electrical and Information Engineering, Hunan University, Hunan, China.

His research interests include electrical measurement, digital signal processing, and calibration of instrument transformers.

Lorenzo Peretto (M'98, SM'03) is currently a Professor of electrical and electronic measurements with the University of Bologna, Bologna, Italy. He has authored or co-authored more than 200 articles, holds 24 patents, and co-authored 3 books. He is a consultant of industries operating in the field of instrumentation and sensors for electrical measurements. His fields of research are the design and calibration of voltage and current instrument transformers (LPIT) for medium- and high-voltage power networks, the design and realization of calibration systems of voltage and current instrument transformers, and the measurements of electrical quantities in power networks.

Dr. Peretto is a member of the IEEE Instrumentation and Measurement Society. He is the Chairman of the Annual IEEE Applied Measurements for Power System Conference, a member of the IEC TC38 "Instrument Transformers," and the Chairman of the TC38/WG45 "Standard Mathematical Models for Instrument Transformers" and the TC38/WG53 "Uncertainty Evaluation in the Calibration of Instrument Transformers."

He Wen (M'12, SM'20) was born in Hunan, China, in 1982. He received the B.Sc., M.Sc, and Ph.D. degrees in electrical engineering from Hunan University, Hunan, China, in 2004, 2007, and 2009, respectively.

He is currently a full professor with the College of Electrical and Information Engineering, Hunan University, China. His present research interests include electrical contact reliability, wireless communications, power system harmonic measurement and analysis, power quality, and digital signal processing. Also, he is the deputy director of Hunan Province Key Laboratory of Intelligent Electrical Measurement and Application Technology.

Dr. Wen is currently an Associate Editor of the IEEE TRANSACTIONS ON INSTRUMENTATION AND MEASUREMENT, Academic Editor of JOURNAL OF SENSORS, Member of Editorial Board of FLUCTUATION AND NOISE LETTERS and CHINA MEASUREMENT AND TEST.